MOLECULAR IMAGING AND BIOLOGY

Mol Imaging Biol (2020) 22:348–357
DOI: 10.1007/s11307-019-01400-y

Published Online: 8 July 2019

RESEARCH ARTICLE

Longitudinal PET Imaging of α7 Nicotinic Acetylcholine Receptors with [^{18}F]ASEM in a Rat Model of Parkinson's Disease

Steven Vetel,[1] Johnny Vercouillie,[1,2] Frédéric Buron,[3] Jackie Vergote,[1] Clovis Tauber,[1] Julie Busson,[1] Gabrielle Chicheri,[1] Sylvain Routier,[3] Sophie Sérrière,[1] Sylvie Chalon[1]

[1]*UMR Inserm U1253, iBrain, Université de Tours, UFR de Médecine, 10 Boulevard Tonnellé, 37032, Tours Cedex 01, France*
[2]*INSERM CIC 1415, University Hospital, Tours, France*
[3]*Institut de Chimie Organique et Analytique, ICOA, UMR CNRS 7311, Université d'Orléans, Orleans, France*

Abstract

Purpose: The nicotinic acetylcholine alpha-7 receptors (α7R) are involved in a number of neuropsychiatric and neurodegenerative brain disorders such as Parkinson's disease (PD). However, their specific pathophysiologic roles are still unclear. In this context, we studied the evolution of these receptors *in vivo* by positron emission tomography (PET) imaging using the recently developed tracer 3-(1,4-diazabicyclo[3.2.2]nonan-4-yl)-6-[^{18}F]fluorodibenzo[*b*,*d*]thiophene-5,5-dioxide) in a rat model mimicking early stages of PD.

Procedures: PET imaging of α7R was performed at 3, 7, and 14 days following a partial striatal unilateral lesion with 6-hydroxydopamine in adult rats. After the last imaging experiments, the status of nigro-striatal dopamine neurons as well as different markers of neuroinflammation was evaluated on brain sections by autoradiographic and immunofluorescent experiments.

Results: We showed an early and transitory rise in α7R expression in the lesioned striatum and substantia nigra, followed by over-expression of several gliosis activation markers in these regions of interest.

Conclusions: These findings support a longitudinally follow-up of α7R in animal models of PD and highlight the requirement to use a potential neuroprotective approach through α7R ligands at the early stages of PD.

Key words: Dopamine neurotransmission, Neurodegeneration, Neuroinflammation, Microglia, M1/M2 phenotype

Introduction

The nicotinic acetylcholine alpha-7 receptors (α7R) are involved in a number of brain disorders, and activation of these receptors has shown beneficial effects on cognitive impairments associated with several neuropsychiatric [1] and neurodegenerative [2–4] diseases. These multiple involvements of α7R are probably related to their localization not only on neurons but also on CNS immune cells where their activation have been shown to reduce the inflammatory processes which are common to rather all brain disorders [5]. In this context, *in vivo* brain exploration of these receptors would be of great value not only to gain greater knowledge of their pathophysiologic role but also to evaluate potential therapeutic drugs targeting them.

Electronic supplementary material The online version of this article (https://doi.org/10.1007/s11307-019-01400-y) contains supplementary material, which is available to authorized users.

Correspondence to: Sylvie Chalon; *e-mail:* sylvie.chalon@univ-tours.fr

A number of attempts have been performed in the last decade to obtain a α7R tracer suitable for positron emission tomography (PET), which is the most efficient method for quantitative *in vivo* molecular imaging. These efforts have encountered a number of difficulties related in particular to the very low density of these receptors in the brain [6, 7]. However, among the candidate PET tracers, 3-(1,4-diazabicyclo[3.2.2]nonan-4-yl)-6-[^{18}F]fluorodibenzo[*b*,*d*]thiophene-5,5-dioxide), or [^{18}F]ASEM, seems to display optimal properties, with a high affinity (Ki = 0.4 nM) and selectivity for α7R, and a specific and adequate accumulation in mouse brain [8]. In addition, this highly promising tracer has recently proven its usefulness for the quantification of α7R in healthy human brain [9, 10] and in schizophrenia [11]. As a complement to clinical imaging studies, the use of animal models provides an important tool in biomedical research, *e.g.*, for investigating the role of different molecular pathways involved in specific pathological processes, as well as for target validation and treatment evaluation. In the case of Parkinson's disease (PD), a treatment that could slow down or stop the neuronal death is still needed. In this context, a better knowledge of the role of α7R in this disease could be of value. We studied here, for the first time, the evolution of α7R by PET imaging in a rat model mimicking early stages of PD.

Materials and Methods

All experimental procedures are summarized in Suppl. Fig. 1 (see Electronic Supplementary Material (ESM)).

Animals

All procedures were conducted in accordance with the requirements of the European Community Council Directive 2010/63/EU for the care of laboratory animals and with the authorization of the Regional Ethical Committee (Authorization No. 2016.022218004689 and No. 00434.02). Experiments were performed on adult male Wistar rats weighing 250–300 g (Janvier, Le Genest-Saint-Isle, France). A total of 21 animals were used (13 rats were used for the *ex vivo* biodistribution studies and 8 rats for 6-hydroxydopamine (6-OHDA) experiments). Rats were kept in a temperature (23 ± 0.5 °C) and humidity (43 ± 8 %) controlled environment under a 12-h light-dark cycle with food and water available *ad libitum*.

Preparation of [^{18}F]ASEM

The synthesis of the stable ASEM and the nitro precursor for radiosynthesis of [^{18}F]ASEM were adapted from Gao et al. [8]. The radiosynthesis was performed on a FXFN® module (GE Healthcare, Upsalla, Sweden). Quaternary ammonium anion exchange (QMA) cartridges and Sep-Pak® light C-18 were provided by Waters (Milford, MA, USA). HPLC purifications were performed on a Zorbax Eclipse XDB-C18 9.4 × 250 mm 5 µ (Agilent®, Santa Clara, CA, USA). Quality control was performed on an Ultimate 3000 HPLC (Thermo, Waltam, MA, USA), equipped with a variable wavelength detector and B-FC-4100 radiodetector (Bioscan, Oxnard, CA, USA) using Zorbax Eclipse XDB-C18 4.6 × 150 mm 5 µ. [^{18}F]-fluorine was sent into the automaton, trapped on the QMA cartridge, and then elution of fluorine was performed with a solution of $K_2CO_3/K_{2.2.2}$. The solution was dried in the reactor under azeotropic atmosphere using two times 1 ml of MeCN. After drying the [^{18}F]fluoride complex, 2 mg of the precursor 3-(1,4-diazabicyclo[3.2.2]nonan-4-yl)-6-nitrodibenzo[*b*,*d*]-thiophene-5,5-dioxide dissolved in 0.8 ml of DMSO was added. The solution was heated at 160 °C for 12 min, then cooled to room temperature (RT), and diluted with 2 ml of water and 1 ml of acetonitrile. Solution was loaded onto the loop and purified on the semi-preparative column using TEA 0.2 %/ACN 60/40 as the mobile phase at 4 ml/min. The collected fraction was diluted in 30 ml of water and trapped on a *t*-C18 light cartridge. Elution from the cartridge was performed with 0.5 ml of ethanol, and the formulation was completed by adding 4.5 ml of 0.9 % NaCl. The tracer was obtained in about 35 % radiochemical yield with a radiochemical purity greater than 95 % and a molar activity of 33.5 ± 5.32 GBq/µmol at the end of production.

Ex vivo Brain Biodistribution Experiments in Healthy Rats

Thirteen rats were included in this experiment and were divided in two experimental groups as follow: six rats in the control group and seven rats in the methyllycaconitine (MLA) group. All rats were injected intravenously (i.v.) under isoflurane gas anesthesia in the penis vein with 0.3 ml of [^{18}F]ASEM (2.20 ± 0.13 MBq). Animals from the control group received only the tracer whereas animals from the MLA group received an i.v. injection of 1 mg/kg MLA (Tocris, R&D Systems Europe, Lille, France) 15 min before the tracer injection. All rats were euthanized by decapitation at 1 h post-injection of the tracer. The whole brain was quickly removed and dissected into areas consisting of the hippocampus, colliculi, prefrontal cortex, thalamus, striatum, and cerebellum. Samples were weighed, radioactivity was measured in a γ-counter (2480 Gamma counter Wizard, PerkinElmer, counting efficiency of 48 % for fluorine-18), and the percent injected dose per gram of tissue (%ID/g) was calculated by comparison with samples to standard dilutions of the injected solution.

6-OHDA Lesion

A striatal unilateral 6-OHDA lesion was performed in 8 rats as described in ESM.

Rotation Test

At 13 days post-lesion (dpl), the rats received an intraperitoneal (i.p.) injection of D-amphetamine sulfate (3 mg/kg) (Sigma-Aldrich, Saint-Quentin Fallavier, France) and were then placed in automatic rotameter bowls (Imetronic, Pessac, France). Starting 15 min after injection, the number of ipsilateral rotations was measured for 2 h. Full rotation was defined as a complete, uninterrupted 360° turn.

PET Imaging of α7R with [^{18}F]ASEM and Data Analyses

PET imaging of α7R with [^{18}F]ASEM was performed at 3, 7, and 14 dpl ($n = 8$). Each animal received an i.v. bolus injection of 37 MBq of [^{18}F]ASEM into the tail vein and was scanned using a microPET-CT SuperArgus system (Sedecal, Madrid, Spain), under isoflurane anesthesia (Baxter, France; 4–5 % in O2 for induction and 1.5–2 % during image acquisition). The rat's head was placed on the center of the field of view (FOV 1–2 mm spatial resolution, 2.5 % sensitivity). A 5-min computed tomography (CT) scan was recorded before PET acquisition for taking into account the attenuation correction. The respiratory rate and body temperature of rats were monitored during the 61 min of PET acquisition. The PET list-mode scans were rebinned into 33 frames: 1 frame of 60 s (before injection of the tracer), followed by 4 frames of 10 s, 4 of 20 s, 4 of 60s, 14 of 180 s, and 6 of 120 s. The quantification of the tracer uptake was extracted from the last 6 frames of 120 s corresponding to 49–61 min of acquisition after tracer injection. Each image was corrected for randoms, scatter, and attenuation and was reconstructed using a 2-dimensional OSEM algorithm (GE Healthcare, France) into voxels of $0.3875 \times 0.3875 \times 0.775$ mm^3. A partial volume effect correction was applied on all images which were co-registered in a single interpolation to the Schiffer rat brain MRI template as described in [12]. PET images were reconstructed and analyzed using PMOD (3.403, PMOD Technologies, Zurich, Switzerland). The regions of interest (ROIs) were the left non-lesioned striatum (contralateral striatum, C-ST), right lesioned striatum (ipsilateral striatum, I-ST), left substantia nigra (contralateral substantia nigra, C-SN), right substantia nigra (ipsilateral substantia nigra, I-SN), and cerebellum (CE). In this study, the standard uptake value ratio (SUVr) was used as quantitative criterion. All SUVrs were calculated using the CE as a reference region.

Autoradiographic and Immunofluorescence Experiments

Brain Tissue Preparation After the last PET imaging scan at 14 dpl, each rat was injected i.p. with a lethal dose of pentobarbital (60 mg/kg, Ceva Santé Animale, France) and trans-cardially perfused with 250 ml of cold sterile physiological water. Then, the brain was removed, frozen in an isopentane/dry ice mixture maintained at − 36 °C and kept at − 80 °C. Sixteen-µm-thick brain sections were cut in the coronal plane at − 20 °C with a cryostat (CM3050S, Leica, Germany), gathered on gelatinized glass slides, and then stored at − 80 °C.

Autoradiography Autoradiographic experiments were performed with the dopamine transporter (DAT) tracer [^{125}I]PE2I which was radiolabeled according to previously described methods [13] and obtained with a molar activity of 95 GBq/µmol. After equilibration at RT for 3 h, brain sections (6 per rat) were incubated for 90 min with 100 pmol/l [^{125}I]PE2I in phosphate buffer pH 7.4. Non-specific binding was measured by adding 100 µmol/l cocaine chlorhydrate (Cooper Industrie, Melun, France) in the incubation medium. After 2 washings of 5 min in 4 °C buffer, the sections were briefly rinced in 4 °C sterile water and dried at RT. Dry sections were then placed in the gas chamber of a β- imager TM 2000 system (Biospace Lab, Paris, France) after application of metal electric tape (3M, Euromedex) on the free side of slides. After 4 h acquisition, the C-ST and I-ST were drawn manually according to the rat brain Atlas of Paxinos and Watson [14]. The level of bound radioactivity was directly determined by counting the number of gamma/X-ray emitted from the delineated areas using the β-vision software (Biospace Lab, Paris, France). The radioactivity in C-ST and I-ST corresponding to the specific binding of the tracer was quantified using an image analyzer (M2-Vision Biospace Instruments) and expressed as counts per minute per square millimeter (cpm/mm^2).

Immunofluorescence Immunostaining was performed on brain sections adjacent to those used for autoradiography. Two single immunostainings were performed, *i.e.*, tyrosine hydroxylase (TH) as a specific marker of dopaminergic neurons in the SN, and glial fibrillary acidic protein (GFAP) as a specific marker of astrocytes, both in the striatum and SN. Double staining of CD11b and P2X7 receptors (P_2X_7R) was performed both in the striatum and SN. CD11b is a membrane marker of monocytes used as a marker of microglial activation, and P_2X_7R is a localized on brain immune cell. All details are provided in the ESM.

Statistical Analyses All results were expressed as means ± standard error means (SEM). Statistical analyses were carried out with the GraphPad Prism software version 6 (San Diego, CA). For *ex vivo* biodistribution experiments, comparisons between the control and MLA groups were performed using the Mann-Whitney test two tailed. For PET imaging in lesioned animals, data were analyzed using a paired Wilcoxon test within subjects over time. For autoradiographic and immunofluorescence analyses, comparisons between C-ST and I-ST and between C-SN and I-

SN were performed using the Wilcoxon test two tailed. For all experiments, the level of significance was set at $p < 0.05$.

Results

Ex vivo brain biodistribution experiments in healthy rats

As shown in Fig. 1, the accumulation of [^{18}F]ASEM at 1 h after i.v. injection was found, from the highest to lowest, in the hippocampus (0.80 ± 0.16 %ID/g tissue), colliculi (0.72 ± 0.15 %ID/g), prefrontal cortex (0.48 ± 0.08 %ID/g), thalamus (0.40 ± 0.07 %ID/g), striatum (0.28 ± 0.03 %ID/g), and cerebellum (0.17 ± 0.02 %ID/g). Pre-injection of the α7R antagonist MLA induced a significant decrease in the accumulation of the tracer in the four first brain structures (− 58 % in the hippocampus, $p = 0.0012$; − 71 % in the colliculi, $p = 0.0012$; − 44 % in the prefrontal cortex, $p = 0.0012$; − 32 % in the thalamus, $p = 0.0047$) and a tendency to decrease in the striatum (− 15 %, $p = 0.073$), whereas no modification was observed in the cerebellum.

Amphetamine-Induced Rotation Test

The amphetamine-induced rotation test was performed at 13 dpl. All animals displayed a turning behavior, with an average of 6.73 ± 0.69 ipsilateral rotations per minute, in agreement with the 6-OHDA lesion.

PET Imaging of α7R

PET imaging of α7R with [^{18}F]ASEM was performed in each animal at 3, 7, and 14 dpl, and quantitative image analysis was carried out in the striatum and SN. The static axial PET images as represented in Fig. 2a were obtained in a same animal at 14 dpl between 30 and 50 min after radiotracer injection. As shown in Fig. 2b and c, the quantitative analysis of SUVr revealed that no statistical significant difference was observed longitudinally, whatever the region (C-ST, I-ST, C-SN, I-SN) and the paired time-point (3 dpl *vs* 7 dpl, 3 dpl *vs* 14 dpl, 7 dpl *vs* 14 dpl). For the comparison between the ipsi- and contralateral sides, a statistical significant increase was observed in the striatum at 3 dpl (0.88 ± 0.05 *vs.* 0.80 ± 0.05 SUVr, $p < 0.05$), but not at 7 and 14 dpl (Fig. 2b), and a statistical significant increase was observed in the SN at 7 dpl (0.90 ± 0.07 *vs.* 0.77 ± 0.06 SUVr, $p < 0.05$), but not at 3 and 14 dpl (Fig. 2c).

Autoradiography

After the last imaging session (14 dpl), the density of striatal DAT was evaluated on each rat's coronal brain sections with [^{125}I]PE2I as illustrated in Fig. 3a and b. According to Fig. 3c, the specific binding of the radioligand was significantly lower (by 71.02 ± 3.17 %) in the I-ST than in the C-ST (6.33 ± 0.55 *vs.* 22.08 ± 0.65 cpm/mm^2, respectively, $p < 0.05$).

Immunofluorescence Experiments

Immunostaining of TH was quantified in the SN on coronal brain sections as illustrated in Fig. 4a. Quantitative measurements (Fig. 4b) showed that the number of TH-positive cells was significantly decrease (by 66.45 ± 2.98 %) in the I-SN compared to the C-SN (18.56 ± 1.91 *vs.* 55.06 ± 3.14 TH-positive cells, respectively, $p < 0.05$).

GFAP immunostaining was performed in both the striatum and SN on coronal brain sections as illustrated in Fig. 5a and c, respectively. In the striatum, the area occupied by GFAP immunostaining was significantly higher (by 81.73 ± 16.50 %) in the I-ST than in the C-ST (8.20 ± 0.65 *vs.* 4.59 ± 0.28 % of stained area, respectively, $p < 0.05$) (Fig. 5b). In the SN (Fig. 5d), the area occupied by GFAP immunostaining was also significantly higher (by 91.90 ± 19.11 %) in the I-SN compared to the C-SN (9.99 ± 0.57 % *vs.* 5.48 ± 0.50 % of stained area, respectively, $p < 0.05$).

Double staining of CD11b and P_2X_7R was assessed on coronal brain sections both in the striatum and SN (Fig. 6a). In the striatum, the number of CD11b-positive cells was significantly higher (by 207.50 ± 26.53 %) in the I-ST compared to the C-ST (16.40 ± 0.83 *vs.* 5.63 ± 0.55 CD11b cells, respectively, $p < 0.05$) (Fig. 6b). Similarly, the number of CD11b/P_2X_7R-positive cells was significantly higher (by 330.48 ± 54.31 %) in the I-ST compared to the C-ST (11.90 ± 0.47 *vs.* 3.04 ± 0.34 CD11b/P_2X_7R cells, respectively, $p < 0.05$) (Fig. 6d). In the SN, as shown in Fig. 6c, the number of CD11b-positive cells was significantly higher (by 187.36 ± 15.40 %) in the I-SN than in the C-SN (12.84 ± 0.89 *vs.* 4.59 ± 0.44 CD11b cells, respectively, $p < 0.05$). In addition, the number of CD11b/P_2X_7R positive-cells was also significantly higher (by 536.08 ± 135.99 %) in the I-SN than in the C-SN (9.19 ± 0.46 *vs.* 1.91 ± 0.46 CD11b/P_2X_7R cells, respectively, $p < 0.05$) (Fig. 6e). In the I-ST and I-SN, the percentages occupied by the number of CD11b/ P_2X_7R cells relative to the total number of CD11b cells were 72.55 % and 71.53 %, respectively.

Discussion

PET exploration of specific molecular brain targets is a powerful approach for the early diagnosis, follow-up, and treatment evaluation of acute and chronic cerebral dysfunctions. In this context, few data are still available regarding *in vivo* imaging of α7R, despite their multiple physiopathological roles [15]. A number of publications have indicated a therapeutic potential of nicotine for several neuropsychiatric and neurodegenerative disorders through effects mediated by α7R, although disappointing results were recently obtained in Alzheimer's disease and schizophrenia clinical

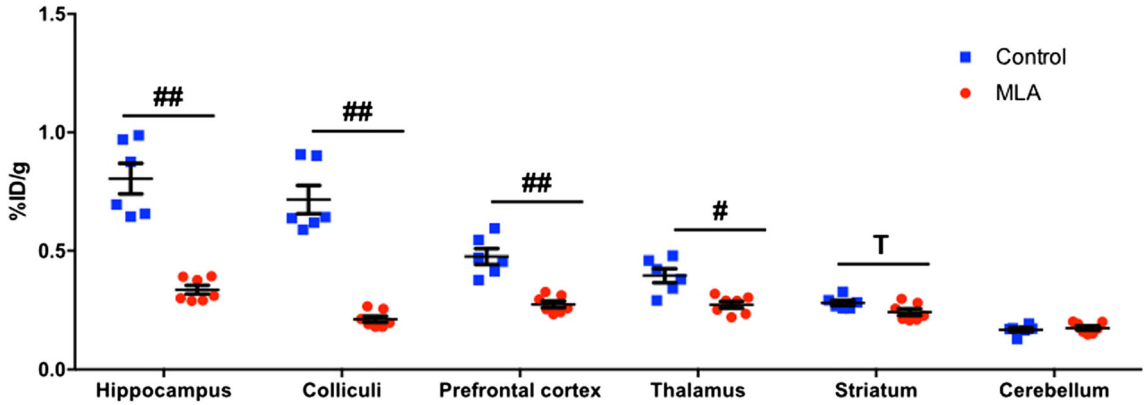

Fig. 1 . *Exvivo* cerebral biodistribution of [^{18}F]ASEM in control rats ($n = 6$) and in animals receiving an intravenous administration of the α7R antagonist methyllycaconitine or MLA ($n = 7$). Accumulation of [^{18}F]ASEM (% injected dose/g tissue) was evaluated in several brain structures including hippocampus, colliculi, prefrontal cortex, thalamus, striatum, and cerebellum. Data are represented as individual points ± SEM. $^{\#\#}p = 0.0012$; $^{\#}p = 0.0047$; T, $p = 0.073$ (two tailed Mann-Whitney test). ID injected dose, MLA methyllycaconitine.

trials using α7R ligands [16]. In the case of PD, some data obtained in animal models indicated protective effects of α7R agonists [4, 12, 17]. However, a better knowledge of the involvement of these receptors in the pathological process could improve our knowledge of this potential therapeutic target. Having the opportunity to explore *in vivo* α7R, we studied, for the first time, the expression profile of these receptors in a rat model mimicking early stages of PD. For this purpose, we used [^{18}F]ASEM, a promising α7R PET imaging tracer recently described [8, 18]. Considering the lack of data on the usefulness of [^{18}F]ASEM for α7R exploration in rats, we first determined the *ex vivo* brain

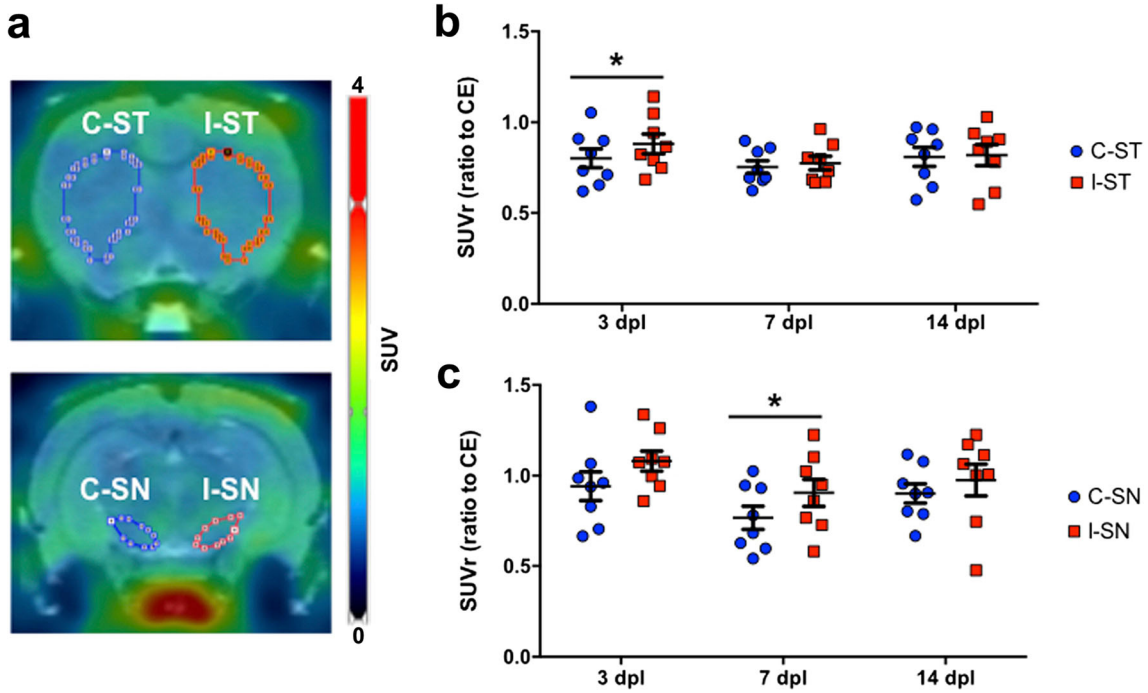

Fig. 2 . PET imaging study: quantification of α7R with [^{18}F]ASEM in 6-OHDA-lesioned rats ($n = 8$). **a** Representative PET brain static coronal images (49–61 min post-injection of the tracer) obtained in a same animal at 14 dpl with [^{18}F]ASEM, co-registered with the MRI-template. Quantitative measurements of SUVrs to CE in **b** C-ST and I-ST and **c** C-SN and I-SN (bottom) measured at 3, 7, and 14 days post-lesion (dpl). Data are represented as individual points ± SEM. $^{*}p < 0.05$ (paired Wilcoxon test). CE cerebellum, C-ST contralateral striatum, I-ST ipsilateral striatum, dpl days post-lesion, C-SN contralateral substantia nigra, I-SN ipsilateral substantia nigra, SUVr standard uptake value ratio to CE.

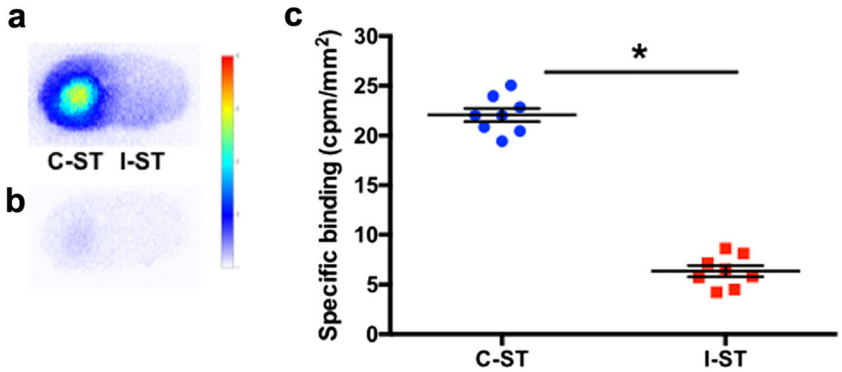

Fig. 3 . Autoradiographic study: quantification of DAT with [^{125}I]PE2I in the striatum of 6-OHDA-lesioned rats ($n = 8$). **a** Representative total and **b** non-specific binding of [^{125}I]PE2I in C-ST and I-ST. **c** Quantitative measurements of DAT density expressed as specific binding of [^{125}I]PE2I (cpm/mm^2) in C-ST and I-ST. Data are represented as individual points ± SEM. *$p < 0.05$ (Wilcoxon test). C-ST contralateral striatum, I-ST ipsilateral striatum.

biodistribution of this radiotracer in this animal species. Our results showed a high uptake of [^{18}F]ASEM in the hippocampus and colliculi, an intermediate uptake in the prefrontal cortex and thalamus, a low uptake in the striatum, and a very low uptake in the cerebellum. This accumulation was strongly reduced in rats that had previously received the α7R antagonist MLA in the high uptake regions, whereas it was slightly reduced in the striatum and no modified in the cerebellum. This confirmed the specificity of the *in vivo* binding of [^{18}F]ASEM, in agreement with the known localization of α7R in rodent brain [19, 20].

In the next experiments, we used a rat model of early stage of PD induced by a partial unilateral 6-OHDA lesion of the nigro-striatal dopaminergic pathway, which we recently characterized [21]. Regarding the complexity of PD, no animal model can reproduce all facets of the human pathology which is characterized by a progressive loss of dopaminergic neurons in the SN *pars compacta* leading to a reduced content of striatal dopamine, a neuroinflammation in both regions, and the presence of abnormal protein aggregates evocative of Lewy bodies [22]. The model we used here is limited in terms of progressive neuronal death and does not show pathological protein inclusions but has the advantage to induce a highly reproducible moderate lesion [21]. The use of buprenorphine as an analgesic just after the lesion is another limitation of the model, as it could interfere with the expression of inflammatory and oxidative markers, although this confounding effect has been observed with a dose 4–5 times higher than that we administrated here [23].

In agreement with our previous findings, we determined that at 14 days after 6-OHDA administration, the nigro-striatal dopaminergic pathway was moderately and

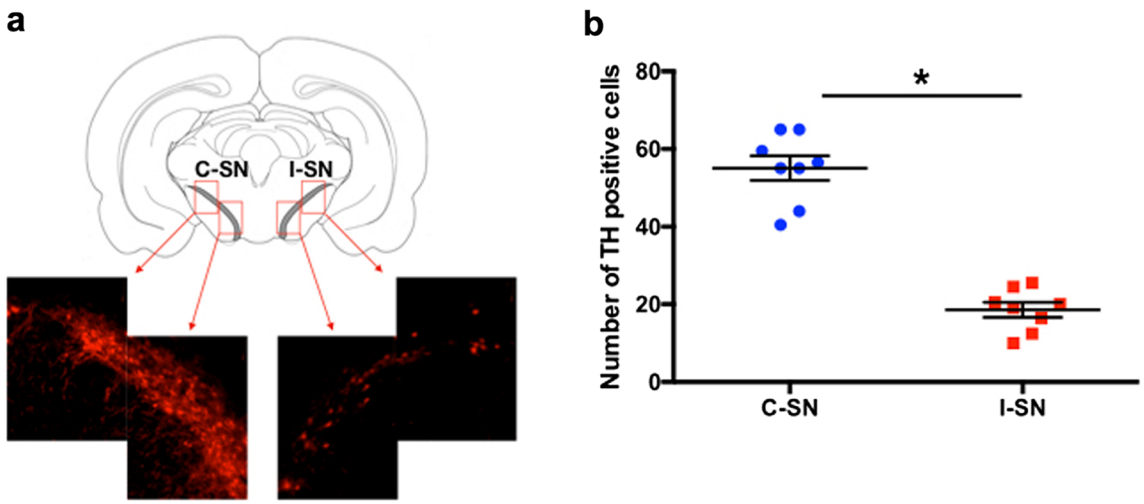

Fig. 4 . Immunofluorescence analysis: quantification of TH in the SN of 6-OHDA lesioned rats (n = 8). **a** Representative immunostaining of TH in C-ST and I-ST. **b** Quantitative measurements of TH positive cells in C-SN and I-SN. Data are represented as individual points ± SEM. *$p < 0.05$ (Wilcoxon test). C-SN contralateral substantia nigra, I-SN ipsilateral substantia nigra, TH tyrosine hydroxylase.

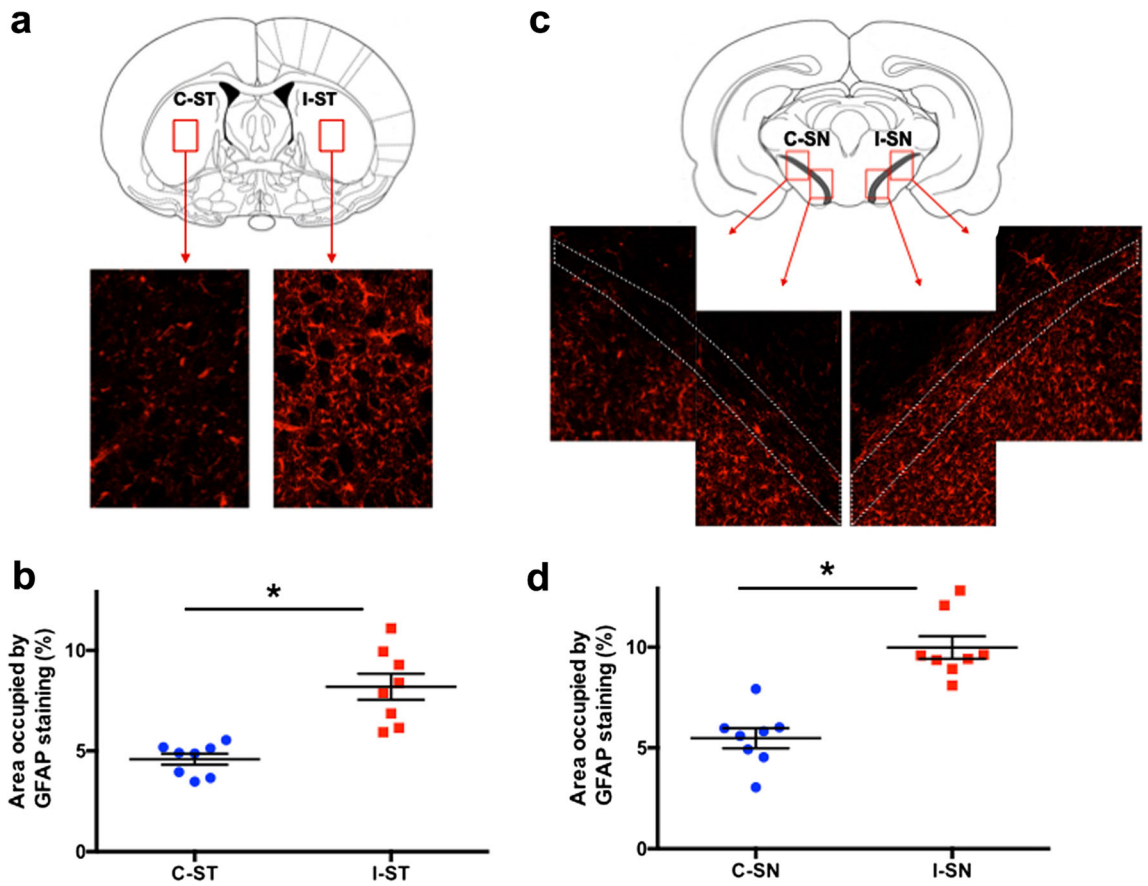

Fig. 5 . Immunofluorescence analysis: quantification of GFAP in the striatum and SN of 6-OHDA-lesioned rats ($n = 8$). **a** Representative immunostaining of GFAP in C-ST and I-ST. **b** Quantitative measurements of area occupied by GFAP staining (%) in C-ST and I-ST. **c** Representative immunostaining of GFAP in C-SN and I-SN. **d** Quantitative measurements of area occupied by GFAP staining (%) in C-SN and I-SN. Data are represented as individual points ± SEM. $^*p < 0.05$ (Wilcoxon test). GFAP glial fibrillary acidic protein, C-ST contralateral striatum, I-ST ipsilateral striatum, C-SN contralateral substantia nigra, I-SN ipsilateral substantia nigra.

reproducibly altered, as demonstrated by a 70 % reduction in the DAT striatal density and a 65 % reduction in the number of TH-positive cells in the SN. The concomitant neuroinflammatory process was assessed by measuring the increased expression of both the CD11b marker of microglial activation and GFAP marker of astrogliosis. At the same time, we showed a rise in the expression of purinergic P_2X_7 receptors (P_2X_7R). These ligand-gated ionotropic receptors activated by ATP and localized on the brain immune cells are involved in the processing and release of pro-inflammatory cytokines [24] and have recently been proposed as potential markers of the M1 (pro-inflammatory) microglia [25, 26].

The longitudinal PET imaging of α7R was performed here in key structures of the nigro-striatal dopaminergic pathway, *i.e.*, the striatum and SN, at 3, 7, and 14 dpl. We observed a significant higher [^{18}F]ASEM binding in the lesioned area compared to the intact side (at 3 dpl only) in the striatum. In the SN ipsilateral to the lesion, a non-statistically significant higher [^{18}F]ASEM binding was observed at 3 dpl, while a statistically significant [^{18}F]ASEM binding occurred at 7 dpl, and no difference was observed at 14 dpl. These last results are probably less accurate than those obtained in the striatum, due to the small size (around 3–5 mm^3) of this brain structure regarding the spatial resolution of the imaging system. Indeed, publications have shown a higher variability and lower reliability of PET quantification with different tracers due to the size of rodent brain regions [27, 28]. Overall, our results showed a transient and early increase in α7R expression following a striatal partial 6-OHDA lesion. It is interesting to note that this increase occurred first in the striatum (3 dpl), *i.e.*, the site of lesion, and then in the SN (7 dpl), as it is known that an intrastriatal administration of 6-OHDA first induces degeneration of dopaminergic nerve endings followed by partial retrograde loss of dopaminergic cell bodies in the SN [29]. Our study has several limitations such as the small number of time points after lesion. In particular, α7R exploration between the lesion and 3 dpl and between 3 and 7 dpl would be of high value. In addition, we compared, at each time point, the level of [^{18}F]ASEM uptake in the lesioned *vs.* intact side of each rat brain and not to a baseline

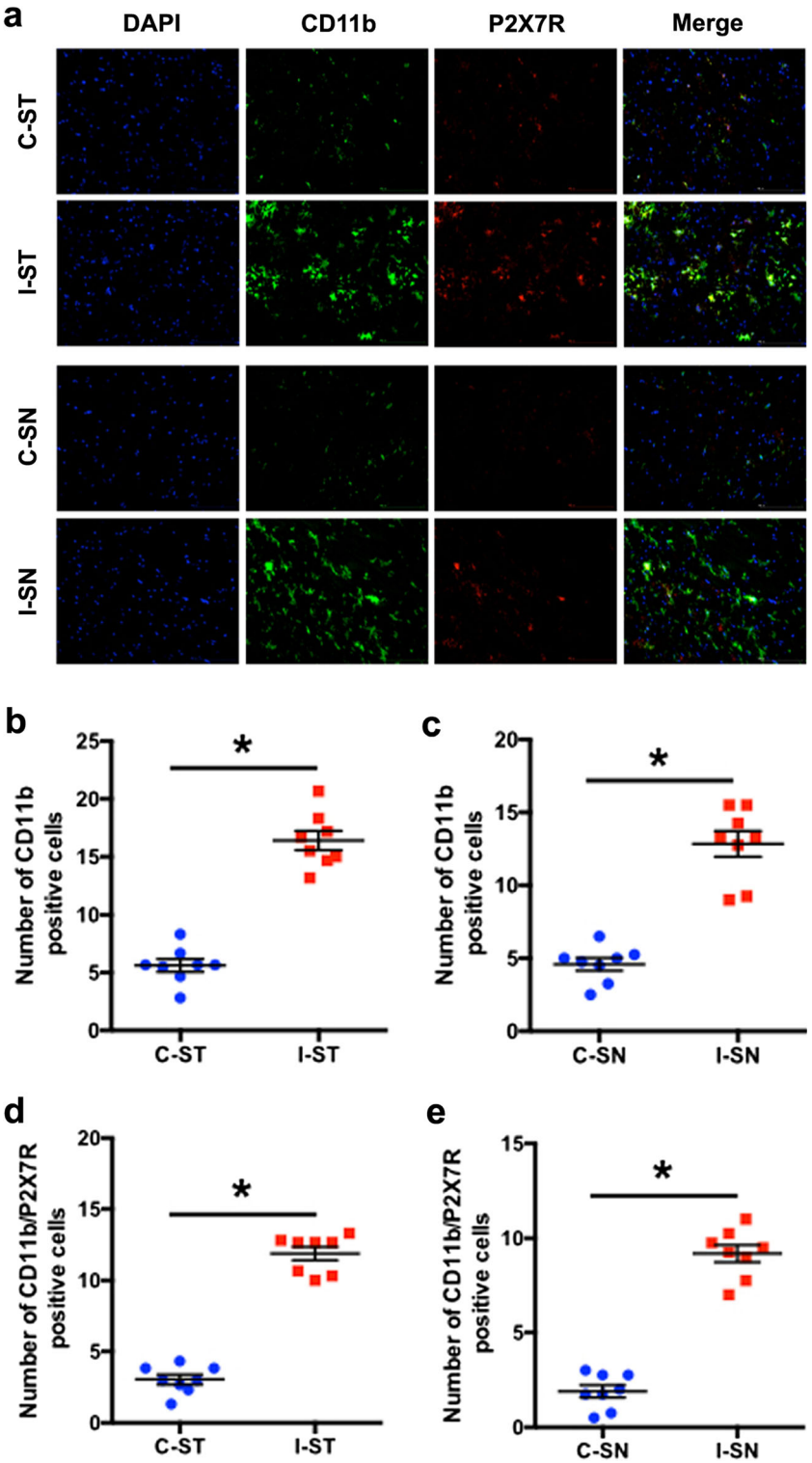

Fig. 6 . Immunofluorescence analysis: quantification of CD11b/P_2X_7R double staining in the striatum and SN of 6-OHDA lesioned rats ($n = 8$). **a** Representative immunostaining of CD11b, P_2X_7R, and DAPI in C-ST and I-ST (upper side) and in C-SN and ISN (lower side). **b** Quantitative measurements of the number of CD11b positive cells in C-ST and I-ST. **c** Quantitative measurements of the number of CD11b positive cells in C-SN and I-SN. **d** Quantitative measurements of the number of CD11b/P_2X_7R positive cells in C-ST and I-ST. **e** Quantitative measurements of the number of CD11b/P_2X_7R positive cells in C-SN and I-SN. Data are represented as individual points ± SEM. $^*p < 0.05$ (Wilcoxon test). P_2X_7R (P_2X_7 receptor), C-ST contralateral striatum, I-ST ipsilateral striatum, C-SN contralateral substantia nigra, I-SN ipsilateral substantia nigra.

measured before lesion. This method could interfere with the result if the unilateral 6-OHDA administration affects the intact side, although the comparison of the lesioned *vs.* intact side is frequently used in this type of unilateral lesion model [21, 22, 29]. In addition, in *in vivo* imaging experiments, the comparison of different brain regions in a same animal offers the advantage to be based on strictly shared experimental conditions regarding the tracer tool (*e.g.*, injected dose, kinetics, metabolism, *etc.*).

Our hypothesis is that the detected α7R could be expressed by activated microglia and/or astrocytes, as already observed *in vitro* after LPS exposure [30] and *post-mortem* in AD human subjects' brain [31]. Several studies have suggested that activation of glial α7R modulates the brain's immune system by promoting the conversion from M1 (inflammatory) to M2 (anti-inflammatory) phenotype [5, 32], and it would be interesting to complete our findings in order to assess whether they could be related to the expression of the M1/M2 activated microglial phenotype. Although we do not have data on the expression of α7R before the 3 dpl stage in this model, we could hypothesize that this early over-expression could be due to a transient response involving M2 microglia. At later stages post-lesion, this tentative neuroprotective response through M2 phenotype could become overwhelmed, in particular because of neuronal death, and could switch into M1 phenotype. In this context, the study of several M1- and M2-phenotype-specific markers during the course of the pathological process would be necessary to reinforce the hypothesis of a biphasic profile of microglial activation in our experimental conditions, as recently described in a rat model close to ours [33]. Although the present data do not allow confirming this hypothesis, this biphasic sequence could occur successively in the striatum and SN, following the retrograde striato-nigral lesion. It can be noted that this kind of pattern of occurrence of M2 and M1 phenotypes has also been described in ischemic conditions [34, 35].

Conclusion

In this study, the PET exploration of α7R with [^{18}F]ASEM was conducted for the first time in a model of PD and showed an over-expression of α7R at early stages after lesion that could reflect a biphasic M2/M1 phenotype of the activated microglia, although this hypothesis remains to be confirmed with complementary experiments. These findings support the use of α7R agonists as an attractive therapeutic approach in PD and highlight its use at the early stages of the disease.

Acknowledgments. We thank the Laboratories Cyclopharma for providing fluor-18 and Sylvie Bodard for technical assistance.

Funding Information. This work was supported by the European Union's Seventh Framework Programme (FP7/2007-2013) under grant agreement No. 278850 (INMiND), by Labex IRON (ANR-11-LABX-18-01), and by the Région Centre-Val de Loire project BIAlz (No. 2014 00091547).

Compliance with Ethical Standards

All procedures were conducted in accordance with the requirements of the European Community Council Directive 2010/63/EU for the care of laboratory animals and with the authorization of the Regional Ethical Committee (Authorization No. 2016.022218004689 and No. 00434.02).

Conflict of Interest

The authors declare that they have no conflict of interest.

References

1. Thomsen MS, Hansen HH, Timmerman DB, Mikkelsen JD (2010) Cognitive improvement by activation of alpha7 nicotinic acetylcholine receptors: from animal models to human pathophysiology. Curr Pharm Des 16:323–343
2. Dineley KT, Pandya AA, Yakel JL (2015) Nicotinic ACh receptors as therapeutic targets in CNS disorders. Trends Pharmacol Sci 36:96–108
3. Fan H, Gu R, Wei D (2015) The alpha7 nAChR selective agonists as drug candidates for Alzheimer's disease. Adv Exp Med Biol 827:353–365
4. Quik M, Zhang D, McGregor M, Bordia T (2015) Alpha7 nicotinic receptors as therapeutic targets for Parkinson's disease. Biochem Pharmacol 97:399–407
5. Kalkman HO, Feuerbach D (2016) Modulatory effects of alpha7 nAChRs on the immune system and its relevance for CNS disorders. Cell Mol Life Sci 73:2511–2530
6. Brust P, Peters D, Deuther-Conrad W (2012) Development of radioligands for the imaging of alpha7 nicotinic acetylcholine receptors with positron emission tomography. Curr Drug Targets 13:594–601
7. Chalon S, Vercouillie J, Guilloteau D, Suzenet F, Routier S (2015) PET tracers for imaging brain alpha7 nicotinic receptors: an update. Chem Commun (Camb) 51:14826–14831
8. Gao Y, Kellar KJ, Yasuda RP, Tran T, Xiao Y, Dannals RF, Horti AG (2013) Derivatives of dibenzothiophene for positron emission tomography imaging of alpha7-nicotinic acetylcholine receptors. J Med Chem 56:7574–7589
9. Hillmer AT, Li S, Zheng MQ, Scheunemann M, Lin SF, Nabulsi N, Holden D, Pracitto R, Labaree D, Ropchan J, Teodoro R, Deuther-Conrad W, Esterlis I, Cosgrove KP, Brust P, Carson RE, Huang Y (2017) PET imaging of alpha7 nicotinic acetylcholine receptors: a comparative study of [^{18}F]ASEM and [^{18}F]DBT-10 in nonhuman primates, and further evaluation of [^{18}F]ASEM in humans. Eur J Nucl Med Mol Imaging 44:1042–1050
10. Coughlin JM, Du Y, Rosenthal HB et al (2018) The distribution of the alpha7 nicotinic acetylcholine receptor in healthy aging: an in vivo positron emission tomography study with [^{18}F]ASEM. Neuroimage 165:118–124
11. Wong DF, Kuwabara H, Horti AG, Roberts JM, Nandi A, Cascella N, Brasic J, Weerts EM, Kitzmiller K, Phan JA, Gapasin L, Sawa A, Valentine H, Wand G, Mishra C, George N, McDonald M, Lesniak W, Holt DP, Azad BB, Dannals RF, Kem W, Freedman R, Gjedde A (2018) Brain PET imaging of alpha7-nAChR with [^{18}F]ASEM: reproducibility, occupancy, receptor density, and changes in schizophrenia. Int J Neuropsychopharmacol 21:656–667
12. Sérrière S, Doméné A, Vercouillie J et al (2015) Assessment of the protection of dopaminergic neurons by an α7 nicotinic receptor agonist, PHA543613 using [^{18}F]LBT-999 in a Parkinson's disease rat model. Front Med 2:61
13. Chalon S, Garreau L, Emond P et al (1999) Pharmacological characterization of (E)-N-(3-iodoprop-2-enyl)-2beta-carbomethoxy-3beta-(4′-methylphenyl)nortropane as a selective and potent inhibitor of the neuronal dopamine transporter. J Pharmacol Exp Ther 291:648–654
14. Paxinos G, Watson C (2009) The rat brain in stereotaxic coordinates. Elsevier Academic Press, San Diego
15. Bertrand D, Chih-Hung LL, Flood D et al (2015) Therapeutic potential of α7 nicotinic acetylcholine receptors. Pharmacol Rev 67:1025–1073

16. Bertrand D, Terry AV (2018) The wonderland of neuronal nicotinic acetylcholine receptors. Biochem Pharmacol 151:214–225
17. Bordia T, McGregor M, Papke RL, Decker MW, Michael McIntosh J, Quik M (2015) The α7 nicotinic receptor agonist ABT-107 protects against nigrostriatal damage in rats with unilateral 6-hydroxydopamine lesions. Exp Neurol 263:277–284
18. Horti AG (2015) Development of [^{18}F]ASEM, a specific radiotracer for quantification of the α7-nAChR with positron-emission tomography. Biochem Pharmacol 97:566–575
19. Clarke PB, Schwartz RD, Paul SM, Pert CB, Pert A (1985) Nicotinic binding in rat brain autoradiographic comparison of [^{3}H]acetylcholine, [^{3}H]nicotine, and [^{125}I]-alpha-bungarotoxin. J Neurosci 5:1307–1345
20. Whiteaker P, Davies AR, Marks MJ et al (1999) An autoradiographic study of the distribution of binding sites for the novel alpha7-selective nicotinic radioligand [^{3}H]-methyllycaconitine in the mouse brain. Eur J Neurosci 11:2689–2696
21. Vetel S, Serriere S, Vercouillie J et al (2019) Extensive exploration of a novel rat model of Parkinson's disease using partial 6-hydroxydopamine lesion of dopaminergic neurons suggests new therapeutic approaches. Synapse 73:e22077
22. Vingill S, Connor-Robson N, Wade-Martins R (2017) Are rodent models of Parkinson's disease behaving as they should? Behav Brain Res 352:133–141
23. Hemshekhar M, Anaparti V, Hitchon C, Mookherjee N (2017) Buprenorphine alters inflammatory and oxidative stress molecular markers in arthritis. Mediat Inflamm 2017:2515408
24. Chakfe Y, Seguin R, Antel JP, Morissette C, Malo D, Henderson D, Séguéla P (2002) ADP and AMP induce interleukin-1beta release from microglial cells through activation of ATP-primed P2X7 receptor channels. J Neurosci 22:3061–3069
25. Apolloni S, Amadio S, Parisi C, Matteucci A, Potenza RL, Armida M, Popoli P, D'Ambrosi N, Volonte C (2014) Spinal cord pathology is ameliorated by P2X7 antagonism in a SOD1-mutant mouse model of amyotrophic lateral sclerosis. Dis Model Mech 7:1101–1109
26. Higashi Y, Aratake T, Shimizu S, Shimizu T, Nakamura K, Tsuda M, Yawata T, Ueba T, Saito M (2017) Influence of extracellular zinc on M1 microglial activation. Sci Rep 7:43778
27. Casteels C, Vermaelen P, Nuyts J et al (2006) Construction and evaluation of multitracer small-animal PET probabilistic atlases for voxel-based functional mapping of the rat brain. J Nucl Med 47:1858–1866
28. Sérrière S, Tauber C, Vercouillie J, Guilloteau D, Deloye JB, Garreau L, Galineau L, Chalon S (2014) In vivo PET quantification of the dopamine transporter in rat brain with [^{18}F]LBT-999. Nucl Med Biol 41:106–113
29. Sauer H, Oertel WH (1994) Progressive degeneration of nigrostriatal dopamine neurons following intrastriatal terminal lesions with 6-hydroxydopamine: a combined retrograde tracing and immunocytochemical study in the rat. Neuroscience 59:401–415
30. Shytle RD, Mori T, Townsend K, Vendrame M, Sun N, Zeng J, Ehrhart J, Silver AA, Sanberg PR, Tan J (2004) Cholinergic modulation of microglial activation by alpha 7 nicotinic receptors. J Neurochem 89:337–343
31. Teaktong T, Graham A, Court J, Perry R, Jaros E, Johnson M, Hall R, Perry E (2003) Alzheimer's disease is associated with a selective increase in alpha7 nicotinic acetylcholine receptor immunoreactivity in astrocytes. Glia 41:207–211
32. Zhang Q, Lu Y, Bian H et al (2017) Activation of the alpha7 nicotinic receptor promotes lipopolysaccharide-induced conversion of M1 microglia to M2. Am J Transl Res 9:971–985
33. Ambrosi G, Kustrimovic N, Siani F, Rasini E, Cerri S, Ghezzi C, Dicorato G, Caputo S, Marino F, Cosentino M, Blandini F (2017) Complex changes in the innate and adaptive immunity accompany progressive degeneration of the nigrostriatal pathway induced by Intrastriatal injection of 6-hydroxydopamine in the rat. Neurotox Res 32:71–81
34. Perego C, Fumagalli S, De Simoni MG (2011) Temporal pattern of expression and colocalization of microglia/macrophage phenotype markers following brain ischemic injury in mice. J Neuroinflammation 8:174
35. Hu X, Li P, Guo Y, Wang H, Leak RK, Chen S, Gao Y, Chen J (2012) Microglia/macrophage polarization dynamics reveal novel mechanism of injury expansion after focal cerebral ischemia. Stroke 43:3063–3070